BIOCHEMISTRY
including biophysical chemistry & molecular biology

Article

pubs.acs.org/biochemistry

Structure Analysis and Comparative Characterization of the Cytochrome *c*′ and Flavocytochrome *c* from Thermophilic Purple Photosynthetic Bacterium *Thermochromatium tepidum*

Yu Hirano,[†,‡,#] Yukihiro Kimura,[§,#] Hideaki Suzuki,[†] Kunio Miki,*[,‡] and Zheng-Yu Wang*[,†]

[†]Faculty of Science, Ibaraki University, Mito 310-8512, Japan

[‡]Department of Chemistry, Graduate School of Science, Kyoto University, Sakyo-ku, Kyoto 606-8502, Japan

[§]Organization of Advanced Science and Technology, Kobe University, Nada, Kobe 657-8501, Japan

Supporting Information

ABSTRACT: The thermodynamic and spectroscopic properties of two soluble electron transport proteins, cytochrome (Cyt) *c*′ and flavocytochrome *c*, isolated from thermophilic purple sulfur bacterium *Thermochromatium* (*Tch.*) *tepidum* were examined and compared with those of the corresponding proteins from a closely related mesophilic bacterium *Allochromatium* (*Alc.*) *vinosum*. These proteins share sequence identities of 82% for the cytochromes *c*′ and 86% for the flavocytochromes *c*. Crystal structures of the two proteins have been determined at high resolutions. Differential scanning calorimetry and denaturing experiments show that both proteins from *Tch. tepidum* are thermally and structurally much more stable than their mesophilic counterparts. The denaturation temperature of *Tch. tepidum* Cyt *c*′ was 22 °C higher than that of *Alc. vinosum* Cyt *c*′, and the midpoints of denaturation using guanidine hydrochloride were 2.0 and 1.2 M for the *Tch. tepidum* and *Alc. vinosum* flavocytochromes *c*, respectively. The enhanced stabilities can be interpreted on the basis of the structural and sequence information obtained in this study: increased number of hydrogen bonds formed between main chain nitrogen and oxygen atoms, more compact structures and reduced number of glycine residues. Many residues with large side chains in *Alc. vinosum* Cyt *c*′ are substituted by alanines in *Tch. tepidum* Cyt *c*′. Both proteins from *Tch. tepidum* exhibit high structural similarities to their counterparts from *Alc. vinosum*, and the different residues between the corresponding proteins are mainly located on the surface and exposed to the solvent. Water molecules are found in the heme vicinity of *Tch. tepidum* Cyt *c*′ and form hydrogen bonds with the heme ligand and C-terminal charged residues. Similar bound waters are also found in the vicinity of one heme group in the diheme subunit of *Tch. tepidum* flavocytochrome *c*. Electron density map of the *Tch. tepidum* flavocytochrome *c* clearly revealed the presence of disulfur atoms positioned between two cysteine residues at the active site near the FAD prosthetic group. The result strongly suggests that flavocytochrome *c* is involved in the sulfide oxidation *in vivo*. Detailed discussion is given on the relationships between the crystal structures and the spectroscopic properties observed for these proteins.

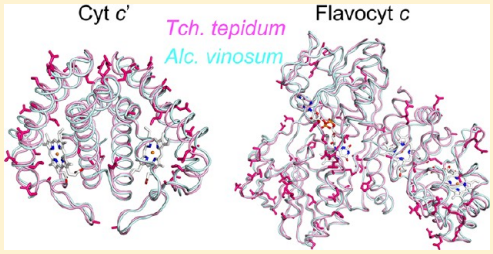

Thermochromatium (*Tch.*) *tepidum* is a thermophilic purple sulfur photosynthetic bacterium originally isolated from a hot spring in Yellowstone National Park.[1] It can grow anaerobically at optimum temperatures of 48−50 °C with an upper limit of 58 °C. A number of proteins purified from this organism have been shown to be thermally more stable compared to their mesophilic counterparts. These include light-harvesting-reaction center core complex (LH1-RC),[2] ribulose-1,5-bisphosphate carboxylase/oxygenase,[3,4] flavocytochrome *c*,[5] and a high-potential iron−sulfur protein (HiPIP).[6,7] While the enhanced thermal stability of the LH1-RC membrane protein was demonstrated to require Ca^{2+} as a cofactor, little is known on the mechanism of the thermostability for other soluble proteins. This is mainly due to the lack of sequence and structural information on these proteins except for the HiPIP. About 90% amino acid identity was found between the HiPIPs from *Tch. tepidum* and its closely related mesophilic bacterium *Allochromatium* (*Alc.*) *vinosum*. The difference in thermostability was attributed to subtle differences in the amino acid sequence and structure.[8]

Cytochrome (Cyt) *c*′ is a *c*-type cytochrome with a pentacoordinated heme that is covalently bound to the C-terminus of the approximately 130-residue polypeptide chain. The Cyt *c*′ homologues are found in a wide variety of bacteria with different metabolic pathways including photosynthetic, denitrifying, and nitrogen fixing as well as methanotrophic and sulfur oxidizing activities,[9] but the physiologic role of Cyt *c*′ is not well understood. It has long been assumed that the Cyt *c*′ is involved in electron transfer and maintaining redox potential.[10,11] Cyt *c*′ can also bind neutral ligands such as CO, NO,

Received: April 30, 2012
Revised: July 17, 2012
Published: July 24, 2012

and alkylisocyanides,[12−15] as well as anionic ligands such as CN^-.[16,17] Although the sequence similarity between the Cyt *c*′ homologues is quite low (~28%),[18] their overall structures are quite similar and can be characterized by a common motif of four-helix bundle.[19] The amino acid sequence of *Alc. vinosum* Cyt *c*′ is featured by the existence of a Tyr16 in helix I which is substituted by Met, Leu, or Phe in the cytochromes *c*′ of other species. The Tyr16 side-chain is parallel to the heme plane and located directly above the sixth ligand site of the heme iron.[20] Ligand binding to this site is expected to cause conformational changes of the helix I, which explains the dimer dissociation of *Alc. vinosum* Cyt *c*′ upon ligand binding.

Flavocytochrome *c*, also known as flavocytochrome *c* sulfide dehydrogenase (FCSD), is involved in sulfide oxidation in both purple and green sulfur photosynthetic bacteria.[21−23] This protein consists of a diheme *c*-binding subunit (FccA, 21 kDa) and a FAD-binding subunit (FccB, 46−47 kDa). Although the flavocytochromes *c* were demonstrated *in vitro* to efficiently catalyze electron transfer from sulfide to a variety of small *c*-type cytochromes, its *in vivo* role is not clear because there are some sulfur-utilizing species that lack this protein and an *Alc. vinosum* mutant deficient in this protein still exhibits sulfide oxidation rates similar to those of the wild type.[24] The crystal structure of the flavocytochrome *c* from *Alc. vinosum* shows that the active site of the FAD-binding subunit contains a catalytically important disulfide bridge located above the pyrimidine portion of the flavin ring and a partial conduit is formed for electron transfer from the flavin to one of the heme groups.[25]

In a previous study, we reported preliminary characterization of several electron transport proteins isolated from *Tch. tepidum*.[7] Here, we present results on the high-resolution crystal structures, spectroscopic and thermodynamic analyses of the Cyt *c*′ and flavocytochrome *c* from this bacterium. Enhanced thermal and structural stabilities of the two proteins have been confirmed in comparison with their mesophilic counterparts, and these properties are interpreted on the basis of the sequence and structural information.

MATERIALS AND METHODS

Gene Sequencing. Genomic DNA from *Tch. tepidum* was isolated as previously reported[26] and used as the template. Partial nucleotide sequence of the gene *cycP* encoding the Cyt *c*′ of *Tch. tepidum* was obtained from a fragment (300 bp) amplified by PCR using the primer pair of (forward) 5′-GCCATCGCCAACTCCGGCAT-3′ and (reverse) 5′-GGCGCCGACATCGCCGAAAG-3′ that were designed on the basis of the *Alc. vinosum cycP* gene.[27] The determined partial sequence had 83% identity to that of the *Alc. vinosum cycP*. With the known sequence information, full-length nucleotide sequence of the *Tch. tepidum cycP* gene and its surrounding regions were determined using the RightWalk kit (BEX Inc., Japan) as described elsewhere.[28] A similar procedure was applied to determine the sequences of *fccA* and *fccB* encoding the *Tch. tepidum* flavocytochrome *c*. Among eight primers designed on the basis of the known *Alc. vinosum fccA* sequence,[29] the primer pair with sequences of (forward) 5′-ACAATTGCGCCGGTTGTCAC-3′ and (reverse) 5′-CGA-CATGGCACTTCTCGCAG-3′ yielded a 300-bp fragment with the partial sequence of *Tch. tepidum fccA* (85% identity). Full sequences of the *Tch. tepidum fccA* and *fccB* genes and its surrounding regions were determined by the RightWalk kit.

Culture Conditions and Purification. Cultures of *Tch. tepidum* and *Alc. vinosum* and purification of the native cytochromes *c*′ and flavocytochromes *c* were described previously.[7,30] The eluted proteins from a DEAE column were further purified by ammonium sulfate precipitation. The cytochromes *c*′ were contained in the supernatant of 70% (w/v) saturated ammonium sulfate and were repeatedly concentrated and diluted with 20 mM Tris-HCl (pH 8.0) buffer using a Centricon YM-30 filter (Millipore) to remove the salt. The flavocytochromes *c* were precipitated in 70−90% saturated ammonium sulfate and were resuspended in 20 mM Tris-HCl (pH 8.0) buffer, followed by extensive washing using the Centricon YM-30 filter.

Spectroscopic Measurements. Absorption spectra were recorded as described elsewhere.[7] Changes in tryptophan fluorescence upon addition of guanidine hydrochloride (GuHCl) were monitored with an RF-5300PC spectrofluorophotometer (Shimadzu) using a 1-cm quartz cuvette. The excitation wavelength was set at 290 nm. Mass spectra were measured on a 4800 Plus MALDI TOF/TOF Analyzer (Applied Biosystems, MDS SCIEX).[28] Resonance Raman (RR) spectra were recorded on a HoloProbe Raman spectrograph (Kaiser optical systems) at room temperature as described previously.[31] Sample concentration was adjusted to 0.44−0.74 mg/mL for cytochromes *c*′ and 1.57−1.63 mg/mL for flavocytochromes *c* using Amicon Ultra 3K in a buffer containing 20 mM Tris-HCl (pH 8.0). Each spectrum was obtained using the fresh samples to minimize laser-induced degradation. Three spectra from different samples were averaged.

Differential Scanning Calorimetry (DSC). DSC measurements were conducted on a nanoDSC II calorimeter (Model 6100, Calorimetry Science Co.) at a heating rate of 0.5 °C/min.[2] Sample solutions of the cytochromes *c*′ and flavocytochromes *c* were prepared by the same procedure as that for the RR measurements. The resulting filtrate from the sample preparation was used as a reference buffer for each DSC measurement. All the samples and filtrates were degassed prior to filling the calorimeter cells. The changes in calorimetric enthalpy ΔH and entropy ΔS at denaturing temperature T_m were evaluated using CpCalc software (Calorimetry Science Co.).[32]

Crystallization and X-ray Diffraction Experiments. Cyt *c*′ purified from *Tch. tepidum* was concentrated to OD_{400} of 20. Crystallization of the Cyt *c*′ was performed using the sitting-drop vapor-diffusion method at 20 °C by mixing 1 μL of protein solution with an equal volume of the reservoir solution containing 0.1 M cadmium chloride, 30% (v/v) PEG400, and 0.1 M sodium acetate (pH 4.0). Flavocytochrome *c* purified from *Tch. tepidum* was concentrated to OD_{410} of 40. Crystallization of the flavocytochrome *c* was performed using the sitting-drop vapor-diffusion method at 20 °C. One microliter of protein solution was mixed with 1 μL of the reservoir solution containing 0.2 M potassium nitrate, 18% (w/v) PEG3000, and 50 mM MES-NaOH (pH 6.0). For X-ray diffraction experiments, the crystals of Cyt *c*′ were mounted in nylon loops and flash frozen in liquid nitrogen. The crystals of flavocytochrome *c* were transferred into the cryoprotectant solution containing the reservoir solution supplemented with 15% (v/v) glycerol, and then flash frozen in liquid nitrogen. X-ray diffraction data were collected at the beamline AR-NW12A of Photon Factory, Tsukuba, Japan. The diffraction data were integrated and scaled using the *HKL2000* program package.[33]

dx.doi.org/10.1021/bi3005522 | *Biochemistry* 2012, 51, 6556−6567

Phasing and Refinement. Structure determination of the Cyt *c*′ and flavocytochrome *c* was performed by the molecular replacement method using the *Molrep* program.[34] The search models used were the crystal structures of Cyt *c*′ (PDB ID 1BBH)[20] and flavocytochrome *c* (PDB ID 1FCD)[25] both from *Alc. vinosum* with the prosthetic groups and solvent molecules removed. Five percent of reflections were used for the free *R* factor calculation in the structure refinement of Cyt *c*′ and flavocytochrome *c*. The initial model of Cyt *c*′ was subjected to rigid body refinement with the *Refmac5* program[35] in a resolution range of 8−1.0 Å. Incorporation of heme groups and modification of the model were performed using the *Coot* program.[36] Positional and isotropic displacement parameters were refined in the resolution range of 50−1.0 Å. After solvent molecules were included in the model, anisotropic displacement parameters were refined and the final model was refined to R_{work} = 13.0% and R_{free} = 15.4%. The refinement of flavocytochrome *c* was started using the rigid body refinement procedure with the *Refmac5* program in a resolution range of 8−1.5 Å. Incorporation of prosthetic groups and modification of the model were performed using the *Coot* program. Positional and isotropic displacement parameters were refined in the resolution range of 50−1.5 Å. Solvent molecules were included in the model, and the final model was refined to R_{work} = 16.0%, R_{free} = 19.5%. Coordinates of the crystal structures of the Cyt *c*′ and flavocytochrome *c* have been deposited in Protein Data Bank under accession codes 3VRC and 3VRD, respectively. The quality of the structures were analyzed using *MolProbity*.[37] Figures were prepared using the *Pymol* program.[38]

RESULTS

The nucleotide sequences determined for the *cycP*, *fccA*, and *fccB* of *Tch. tepidum* are 82%, 84%, and 84% identical with those of the corresponding genes from *Alc. vinosum*, respectively. The amino acid sequences of *Tch. tepidum* Cyt *c*′ and flavocytochrome *c* deduced from the nucleotide sequences are shown in Figure 1 and aligned with those of the corresponding proteins from *Alc. vinosum*. Both proteins from the two bacteria have the same numbers of amino acid residue for each pair and reveal high sequence similarities with 82% identity for the Cyt *c*′ and 86% identity for the flavocytochrome *c*. The nascent *Tch. tepidum* Cyt *c*′ consists of 154 residues with the first 23 residues as a signal peptide and the remaining 131 residues as the mature protein. The molecular weight of the mature Cyt *c*′ was confirmed by TOF/MS measurements. Several features in the composition of amino acid of the mature Cyt *c*′ can be deduced from the sequence information. Many residues with larger side chains in *Alc. vinosum* were substituted to the residues with shorter ones in *Tch. tepidum*. This includes substitutions of 9 residues in *Alc. vinosum* to Ala in *Tch. tepidum* among the 24 different residues. The number of Gly that is considered to contribute to the flexibility of main chain of the protein was decreased in the *Tch. tepidum* Cyt *c*′. The nascent FccA and FccB subunits begin with 25- and 30-residue signal peptides, respectively, followed by the mature forms of 175 residues for FccA and 401 residues for FccB. There is a decrease of total eight Gly residues for the flavocytochrome *c* of *Tch. tepidum* compared to that of *Alc. vinosum*. Two open reading frames coding for a tetraheme Cyt *c* (partial sequence) and an ankyrin homologue (complete sequence) in the upstream of *fccA* were also sequenced. The nucleotide sequences of *cycP*, *fccA*, and *fccB*, along with those of their surrounding regions, have been deposited to the DDBJ databases with the accession numbers AB519153 and AB530491.

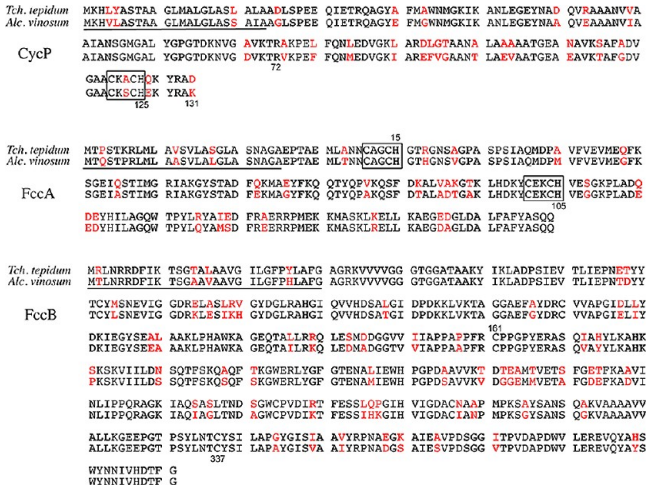

Figure 1. Alignments of the full amino acid sequences of *Tch. tepidum* Cyt *c*′ and flavocytochrome *c* deduced from the nucleotide sequences with those of corresponding proteins from *Alc. vinosum*. Red letters represent different amino acids. Signal sequences are underlined and the heme-binding motifs are indicated by boxes. The numbers refer to those of the amino acid residues in the matured proteins which are mentioned in the text.

Absorption and magnetic circular dichroism spectra of both oxidized and reduced Cyt *c*′ and flavocytochrome *c* from *Tch. tepidum* were reported previously.[7] Here, we present RR spectra of the air-oxidized Cyt *c*′ and flavocytochrome *c* from *Tch. tepidum* and *Alc. vinosum* in the 1800−1100 cm^{-1} region (Figure 2). Most of the *Q*-band RR modes were assigned to the porphyrin in-plane vibrational modes, some of which are sensitive to the chemical property of the heme iron.[39,40] The bands ν_{11} and ν_{19} are RR marker bands for the oxidation and spin states of the heme iron, respectively, and the ν_{10} band is

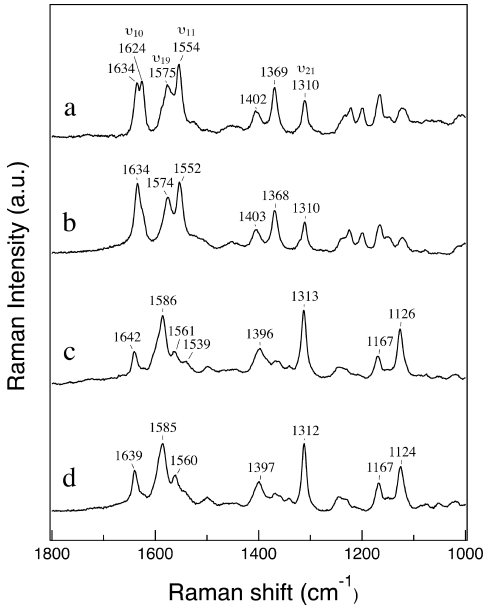

Figure 2. RR spectra obtained by the *Q*-band excitation at 532 nm: (a) *Tch. tepidum* Cyt *c*′, (b) *Alc. vinosum* Cyt *c*′, (c) *Tch. tepidum* flavocytochrome *c*, and (d) *Alc. vinosum* flavocytochrome *c*.

dx.doi.org/10.1021/bi3005522 | *Biochemistry* 2012, 51, 6556−6567

sensitive to both states.[39] The RR spectra of both cytochromes c' were quite similar except for the ν_{10} mode in the 1635−1625 cm^{-1} region where a split band appeared for the *Tch. tepidum* Cyt c' (spectrum a) but a singlet-like band for the *Alc. vinosum* Cyt c' (spectrum b). The frequencies indicate that both cytochromes c' are attributed to a pentacoordinated intermediate-spin (IS) and/or high-spin (HS) states. For the flavocytochromes c (spectra c and d), no RR band was observed from the FAD-binding subunit. The RR bands at 1642 (ν_{10}), 1586 (ν_{19}), 1561 (ν_{11}), and 1313 (ν_{21}) cm^{-1} are all characteristic of a hexacoordinated low-spin cytochrome. The high similarity in the RR spectra suggests that the chemical properties and environment of the heme irons are almost identical for the flavocytochromes c from the two species.

Figure 3 shows the DSC thermograms of cytochromes c' and flavocytochromes c from *Tch. tepidum* and *Alc. vinosum* in the

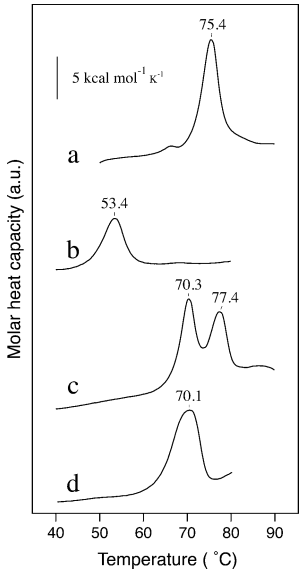

Figure 3. DSC thermograms of cytochromes c' and flavocytochromes c from *Tch. tepidum* and *Alc. vinosum*: (a) *Tch. tepidum* Cyt c', (b) *Alc. vinosum* Cyt c', (c) *Tch. tepidum* flavocytochrome c, and (d) *Alc. vinosum* flavocytochrome c. The scan rate was 0.5 °C/min.

air-oxidized state. An intensive and single band was observed for the *Tch. tepidum* Cyt c' with a maximum at 75.4 °C (curve a). The *Alc. vinosum* Cyt c' exhibited a single denaturing peak at 53.4 °C (curve b), 22 °C lower than that of the *Tch. tepidum* Cyt c'. This result clearly shows that *Tch. tepidum* Cyt c' is thermally much more stable than the *Alc. vinosum* Cyt c'. On the other hand, *Tch. tepidum* flavocytochrome c exhibited two DSC peaks at 70.3 and 77.4 °C (curve c), whereas the *Alc. vinosum* flavocytochrome c showed a broad band at 70.1 °C (curve d). Similar differences in the DSC thermograms were observed at different pH values (data not shown). Thermodynamic parameters of the cytochromes c' and flavocytochromes c evaluated from the DSC profiles are summarized in Table 1. Because the DSC profile of *Tch. tepidum* flavocytochrome c consists of two components with different denaturing temperatures, the stronger band at 70.3 °C was used for the estimation. The changes in calorimetric enthalpies ΔH and entropies ΔS for the Cyt c' and flavocytochrome c of *Tch. tepidum* were about 1.3−1.5 times greater than those of the corresponding proteins from *Alc. vinosum*. The results indicate that thermal denaturation of these proteins from *Tch. tepidum* is

Table 1. Thermodynamic Parameters for the Cytochromes c' and Flavocytochromes c from *Tch. tepidum* and *Alc. vinosum*

		T_m (°C)	ΔH (kcal/mol)	ΔS (kcal/K·mol)
Cyt c'	*Tch. tepidum*	75.4	240	0.69
	Alc. vinosum	53.4	156	0.48
flavocytochrome c	*Tch. tepidum*	70.3, 77.4	347	1.0
	Alc. vinosum	70.1	270	0.79

enthalpically unfavorable but entropically favorable compared with those from *Alc. vinosum*.

In order to compare the stability between the two flavocytochromes c, denaturation of these proteins with GuHCl in air-oxidized state was monitored by fluorescence spectra (Figure 4). Denaturing the flavocytochromes c

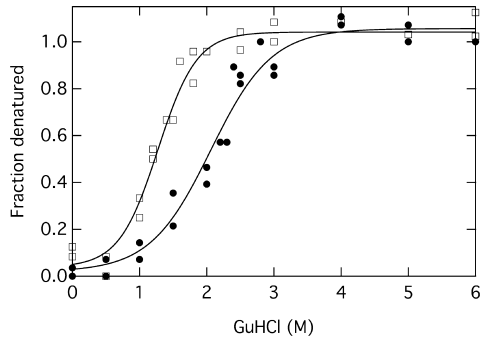

Figure 4. Denaturation curves for the flavocytochromes c from *Tch. tepidum* (closed circles) and *Alc. vinosum* (open squares) generated from the fluorescence emission spectra data. The samples were dissolved in 20 mM Tris-HCl (pH 7.5).

produced large shifts of the emission maxima from 322 to 353 nm, and the denatured fraction was calculated from the emission maximum. Midpoint for the denaturing flavocytochrome c of *Alc. vinosum* was $[GuHCl]_{1/2}$ = 1.2 ± 0.1 M, whereas it was $[GuHCl]_{1/2}$ = 2.0 ± 0.1 M for the *Tch. tepidum* flavocytochrome c. The result indicates that the flavocytochrome c of *Tch. tepidum* is structurally more stable than that of *Alc. vinosum*. Assuming that the denaturing process is a two-state reversible transition, the difference in Gibbs free energy change upon denaturation between the two flavocytochromes c was estimated to be approximately 4.1 kJ/mol.

Crystal structure of the air-oxidized Cyt c' from *Tch. tepidum* has been determined at 1.0 Å resolution. The crystal of Cyt c' belongs to space group $P2_1$ with the unit cell parameters a = 41.3 Å, b = 57.2 Å, c = 54.2 Å, β = 94.8°. Statistics for the diffraction data and refinement are given in Table 2. Cyt c' forms a homodimer, and each monomer (A and B) consists of a four helix bundle, like other Cyt c' proteins.[19] The dimer of Cyt c' reveals high structural similarity to that of *Alc. vinosum*[20] with a root-mean-square (rms) distance of 1.16 Å for the 254 C^{α} atoms (Figure 5a). The *Tch. tepidum* Cyt c' has 17 additional hydrogen bonds formed between the main chain nitrogen and oxygen atoms compared with the *Alc. vinosum* Cyt c' that has a total of 299 main chain hydrogen bonds. The residues different from *Alc. vinosum* are mainly located at the surface of the protein (Figure 5b). Out of the 24 different residues, 17 residues are exposed to the solvent, and other different residues were not observed at the dimer interface. Three hydrophobic

dx.doi.org/10.1021/bi3005522 | *Biochemistry* 2012, 51, 6556−6567

Table 2. Data Collection and Refinement Statistics for the *Tch. tepidum* Cyt *c′* and Flavocytochrome *c*[a]

	Cyt *c′*	flavocytochrome *c*
Diffraction data		
space group	$P2_1$	$I4$
cell parameters	a = 41.3 Å, b = 57.2 Å, c = 54.2 Å, β = 94.8°	$a = b$ = 140.6 Å, c = 57.7 Å
resolution (Å)	50−1.0 (1.02−1.00)	50−1.5 (1.55−1.50)
observed reflections	436902	386975
unique reflections	127655	84166
redundancy	3.4 (2.2)	4.6 (2.9)
R_{merge} (%)[b]	4.0 (21.0)	9.1 (27.8)
$I/\sigma(I)$	42.6 (2.6)	22.6 (3.0)
completeness (%)	94.3 (70.2)	93.4 (84.5)
Refinement		
resolution (Å)	50−1.0	50−1.5
R_{work} (%)[c]	13.0	16.0
R_{free} (%)[c]	15.4	19.5
no. of protein atoms	1989	4385
no. of prosthetic group atoms	91	143
no. of solvent atoms	528	579
rmsd bonds (Å)	0.02	0.03
rmsd angles (°)	2.49	2.74
Ramachandran plot (%)[d]	98.8/1.2/0.0	98.6/1.4/0.0

[a]Values in parentheses represent the highest resolution shell. [b]$R_{merge} = \Sigma_{hkl}\Sigma_i|I_{hkl,i} - \langle I_{hkl}\rangle|/\Sigma_{hkl}\Sigma_i|I_{hkl}|$, where I_{hkl} is the ith measured diffraction intensity and $\langle I_{hkl}\rangle$ is the average of the intensity. [c]$R = \Sigma||F_o| - |F_c||/\Sigma|F_o|$. [d]Favored/allowed/disallowed regions.

residues surrounding the heme group have shorter side chains in *Tch. tepidum* Cyt *c′*; therefore, the helix III in *Tch. tepidum* Cyt *c′* moves closer to the heme group (Figure 5c). Although the helix movement makes the overall fold of *Tch. tepidum* Cyt *c′* shrinking compared with that of *Alc. vinosum* Cyt *c′*, the area of solvent accessible surface for the *Tch. tepidum* Cyt *c′* (9102 Å^2) is slightly larger than that of *Alc. vinosum* Cyt *c′* (8980 Å^2). Because Cyt *c′* is a small protein, the accessible surface area is influenced by small structural changes, such as conformational changes of amino acid residues induced by the crystal packing. The compactness of protein structure has been known as an important factor contributing to the protein stability.[41] The heme group is exposed to solvent at the pyrrole ring IV, and the 18^1 methyl group is accessible to the solvent region (Figure 5d). This was also confirmed by solution NMR using the paramagnetic metal ion (data not shown).

In the crystal structure of *Tch. tepidum* Cyt *c′*, the distances from the axial ligand His125 $N^{\varepsilon 2}$ (the residue number refers to that in the matured proteins and hereinafter) to the heme iron are 2.16 Å and 2.12 Å in monomers A and B, respectively (Figure 6a,b). The His125 and a water molecule form a hydrogen bond with distances of 2.95 Å (monomer A) and 2.93 Å (monomer B). The $C^{\delta 1}$ atom of Tyr16 at the sixth coordinate site is the nearest to the heme iron, and the distances between the two atoms are 3.42 Å and 3.24 Å in monomers A and B, respectively. The heme iron atoms displace from the planes consisting of four nitrogen atoms of the tetrapyrrole rings. The iron atoms move toward the histidine ligands, and the distances between the iron atoms and the four-nitrogen planes are 0.10 Å and 0.09 Å in monomers A and B, respectively. The C-terminal residue Asp131 in monomer A (abbreviated as $Asp131^A$, and the same hereinafter) forms a hydrogen bond with the N^{ε} atom

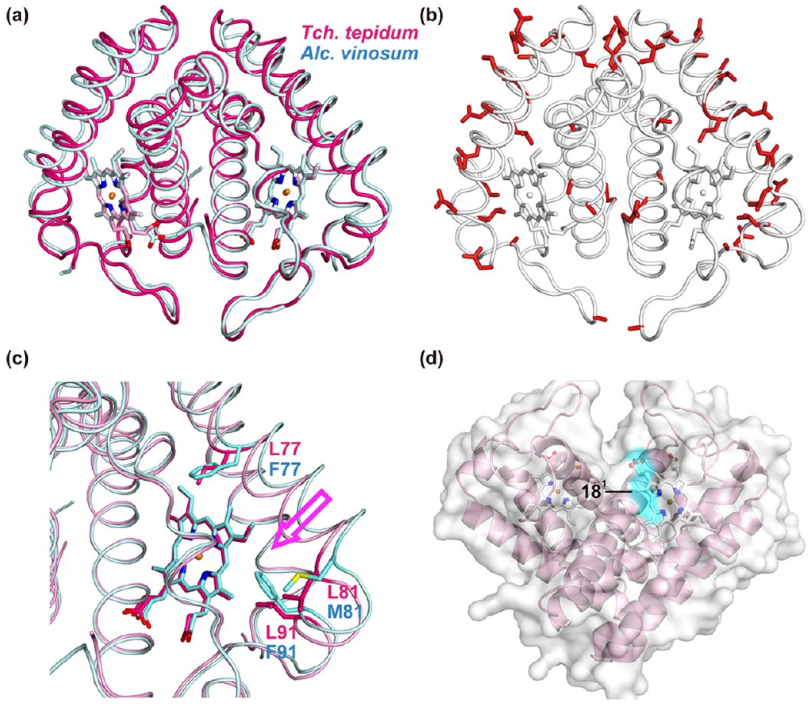

Figure 5. Crystal structure of Cyt *c′*. (a) Superposition between *Tch. tepidum* (pink) and *Alc. vinosum* (blue). (b) Distribution of the different residues between *Tch. tepidum* and *Alc. vinosum*. The different residues were depicted in red sticks displayed on the *Tch. tepidum* Cyt *c′* structure. (c) The residues surrounding the heme groups. The hydrophobic residues different between *Tch. tepidum* and *Alc. vinosum* are shown in sticks. The movement of helix III is indicated with a pink arrow. (d) Surface representation of *Tch. tepidum* Cyt *c′*. The region where the heme group is exposed is colored by blue. The position of the 18^1 methyl group is indicated in the figure.

dx.doi.org/10.1021/bi3005522 | *Biochemistry* 2012, 51, 6556−6567

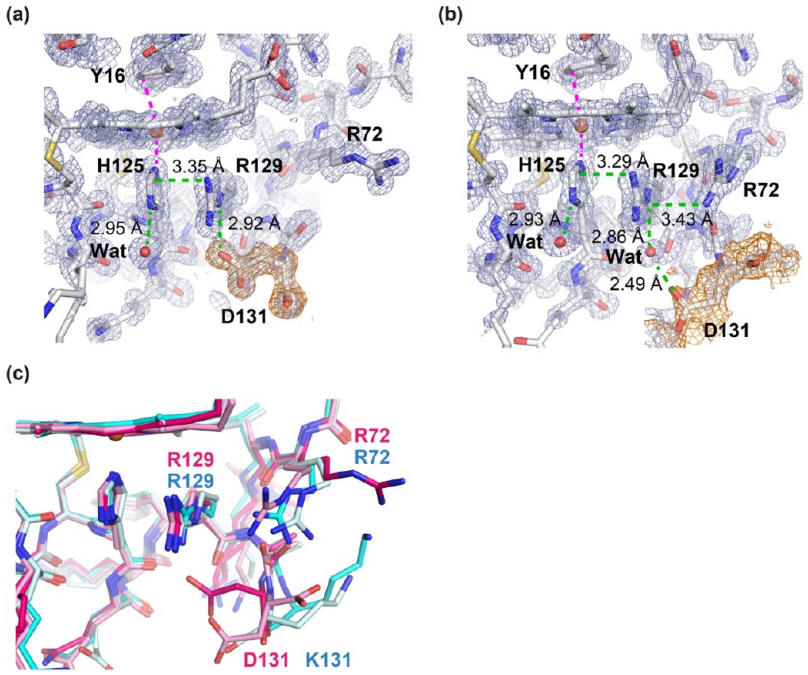

Figure 6. Environment of the histidine axial ligands in *Tch. tepidum* Cyt *c*′. (a) The heme group in monomer A. The $2F_o - F_c$ electron density map is shown as a gray mesh contoured at 1.2σ level and the $F_o - F_c$ omit map of Asp131 is shown as an orange mesh contoured at 3.0σ level. The distances indicated are those of the contacts influencing the His125 ligand field strength. (b) The heme group in monomer B. The $2F_o - F_c$ electron density map is shown as a gray mesh contoured at the 1.2σ level and the $F_o - F_c$ omit map of Asp131 is shown as an orange mesh contoured at the 2.0σ level. (c) Structural comparison between *Tch. tepidum* (pink) and *Alc. vinosum* (blue) around the His125 ligand. The C-terminal residues Asp131 in *Tch. tepidum* and Lys131 in *Alc. vinosum* show the opposite directions of their side chains.

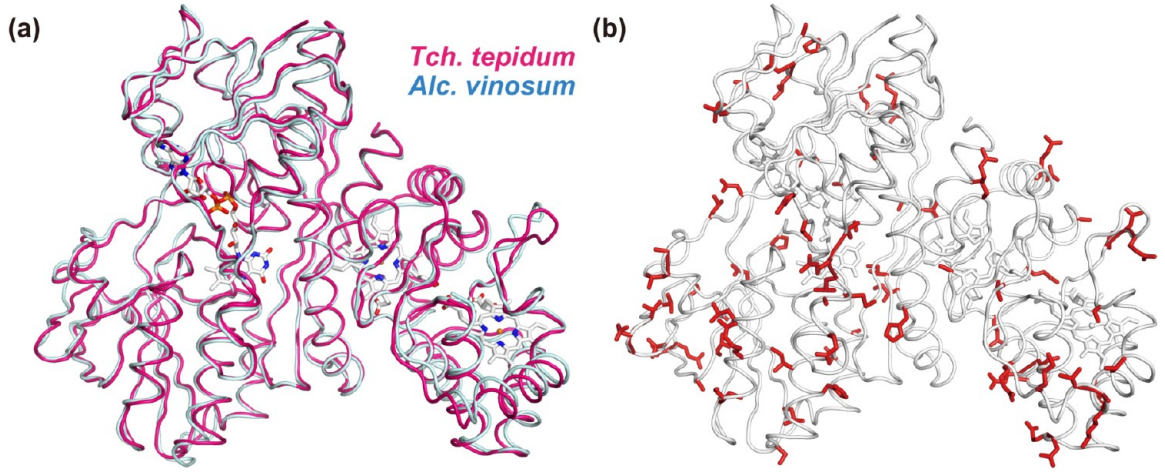

Figure 7. Crystal structure of flavocytochrome *c*. (a) Superposition between *Tch. tepidum* (pink) and *Alc. vinosum* (blue). (b) Distribution of the different residues between *Tch. tepidum* and *Alc. vinosum*. The different residues are shown in red sticks displayed on the *Tch. tepidum* flavocytochrome *c* structure.

of $Arg129^A$ (Figure 6a). The $Arg129^A$ interacts with the axial ligand $His125^A$ via van der Waals contacts. The $Asp131^A$ is fixed by hydrogen bonds with two residues ($Ala36^B$ and $Lys111^A$) of symmetry related molecules in the crystal. The side chain of $Arg72^A$ points toward the solvent region, which is also fixed by hydrogen bonds with two residues ($Leu30^B$ and $Gly32^B$) of a symmetry related molecule in the crystal. On the other hand, the C-terminal residue $Asp131^B$ interacts indirectly with $Arg129^B$ (Figure 6b) via a water molecule that forms hydrogen bonds with both $Asp131^B$ and $Arg129^B$. The $Asp131^B$ is not fixed by crystal packing and its electron density is noisier than that of $Asp131^A$. In contrast to monomer A, the side chain of $Arg72^B$ points toward the $Arg129^B$, and the distance between $Arg72^B$ N^{ω} and $Arg129^B$ N^{ε} is 3.43 Å. The C-terminal residue in *Alc. vinosum* is Lys131 that has opposite charge to that of the Asp131 in *Tch. tepidum*. Therefore, there is no interaction between the Lys131 and Arg129 (Figure 6c). A total of eight cadmium ions were identified in the crystal structure of *Tch. tepidum* Cyt *c*′, and two of them are coordinated by the C-terminal aspartic acid residues of monomers A and B. These metal ions were contained in the crystallization solution. Considering the marked effects of divalent cations on the properties of *Tch. tepidum* LH1 complex,[2] they may also affect

dx.doi.org/10.1021/bi3005522 | *Biochemistry* 2012, 51, 6556−6567

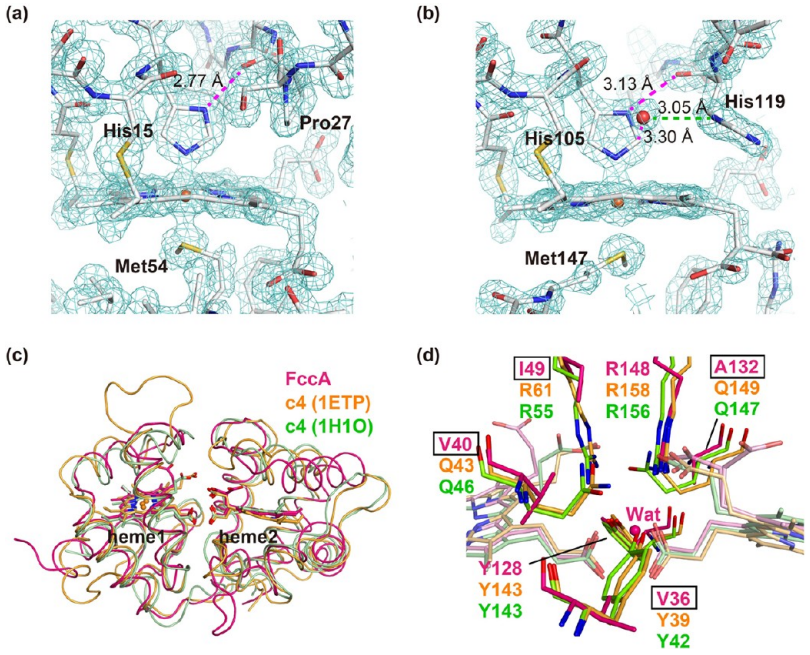

Figure 8. Environment of the heme groups in FccA. (a) Structure around the heme 1 of *Tch. tepidum* flavocytochrome *c*. The $2F_o - F_c$ electron density map is shown as a blue mesh contoured at the 1.5σ level. The hydrogen bond between His15 and Pro27 is indicated by a pink dashed line. (b) Structure around the heme 2 of *Tch. tepidum* flavocytochrome *c*. The $2F_o - F_c$ electron density map is shown as a blue mesh contoured at the 1.5 σ level. The contacts between His105 and His119 or a water are indicated by pink dashed lines, and the hydrogen bond between His119 and a water is in a green dashed line. (c) Superposition between FccA (pink), Cyt c_4 from *Pseudomonas stutzeri* (orange), and Cyt c_4 from *Acidithiobacillus ferrooxidans* (green). (d) A close-up view of (c) around the heme propionates. The residues forming hydrogen bonds with propionates in Cyt c_4 are shown in sticks. The FccA residues different from Cyt c_4 proteins are indicated in boxes. A water molecule located at the position of tyrosine hydroxyl oxygen in Cyt c_4 is shown as a pink sphere.

the thermal stability and/or the ligand field strength of His125 through interaction with the Asp131.

Crystal structure of the air-oxidized flavocytochrome *c* from *Tch. tepidum* has been determined at 1.5 Å resolution. The crystal of flavocytochrome *c* belongs to space group *I*4 with the unit cell parameters $a = b = 140.6$ Å, $c = 57.7$ Å (Table 2). The structure reveals high resemblance to the flavocytochrome *c* from *Alc. vinosum*[25] with a rms distance of 0.94 Å for the 573 C^α atoms (Figure 7a). The *Tch. tepidum* flavocytochrome *c* has 20 additional hydrogen bonds formed between the main chain nitrogen and oxygen atoms compared with *Alc. vinosum* flavocytochrome *c* that has a total of 483 main chain hydrogen bonds. Among the 20 additional hydrogen bonds, only one is observed in FccA, and the other 19 are located in the FccB. The residues different between *Tch. tepidum* and *Alc. vinosum* are mainly located at the protein surface (Figure 7b). Out of the 81 different residues, 62 residues are exposed to the solvent, and the other different residues were not located at the dimer interface. The area of solvent accessible surface for the *Tch. tepidum* flavocytochrome *c* (14430 $Å^2$) is approximately 600 $Å^2$ smaller than that of *Alc. vinosum* flavocytochrome *c* (15096 $Å^2$). In the FccA subunit, two heme groups (heme 1 and 2) are related by a pseudo-2-fold symmetry. The iron atoms of the heme groups are hexacoordinated by the axial ligand residues of histidines (His15 and His105) and methionines (Met54 and Met147) (Figure 8a,b). The distances from the heme 1 iron atom to His15 $N^{\varepsilon 2}$ and Met54 S^γ are 1.98 Å and 2.31 Å, and the heme 2 iron atom to His105 $N^{\varepsilon 2}$ and Met147 S^γ are 2.02 Å and 2.37 Å. His15 forms a hydrogen bond with Pro27. His105 and His119 are also hydrogen bonded, but the distance is longer than that between His15 and Pro27.

An obvious difference between the axial histidine residues in *Tch. tepidum* flavocytochrome *c* is the presence of water molecules in the vicinity of His105. The distance between His105 $C^{\varepsilon 1}$ and the nearest water is 3.30 Å, and the $N^{\delta 1}$–$C^{\varepsilon 1}$–water angle is 87.0° (Figure 8b). The FccA subunit exhibits structural similarities to the cytochrome c_4 proteins from *Pseudomonas stutzeri* (PDB ID: 1ETP)[42] and from *Acidithiobacillus ferrooxidans* (PDB ID: 1H1O)[43] (Figure 8c). Superposition of the secondary structures between the FccA and Cyt c_4 proteins gave the rms distance of 1.87 Å for the 146 C^α atoms of FccA-1ETP and 2.09 Å for the 141 C^α atoms of FccA-1H1O. While overall fold and heme positions are superimposed well, the residues around the heme propionates are different between the FccA and Cyt c_4 proteins (Figure 8d). In Cyt c_4, the arginine and glutamine residues are involved in hydrogen bonds with the heme propionate groups. In contrast, these hydrogen bonds in FccA are lost because the charged residues are replaced by the hydrophobic and shorter residues (Val40, Ile49, Ala132) at the corresponding positions. The two heme groups form direct interaction through one of the propionates in each heme. In Cyt c_4, the hydroxyl groups of two tyrosine residues make hydrogen bond contacts with the propionate groups. One of the tyrosines is substituted to valine (V36) in FccA, and a water molecule is located instead of the hydroxyl oxygen of the tyrosines in Cyt c_4. The water molecule forms a hydrogen bond network with other waters and amino acid residues, which connects to the external solvent region of the protein.

In the FAD binding site of FccB, clear electron densities revealed structural differences between *Tch. tepidum* and *Alc. vinosum*. In *Alc. vinosum*, two cysteine residues (Cys161 and Cys337) form a disulfide bond at the re-side of the FAD. When

dx.doi.org/10.1021/bi3005522 | *Biochemistry* 2012, 51, 6556–6567

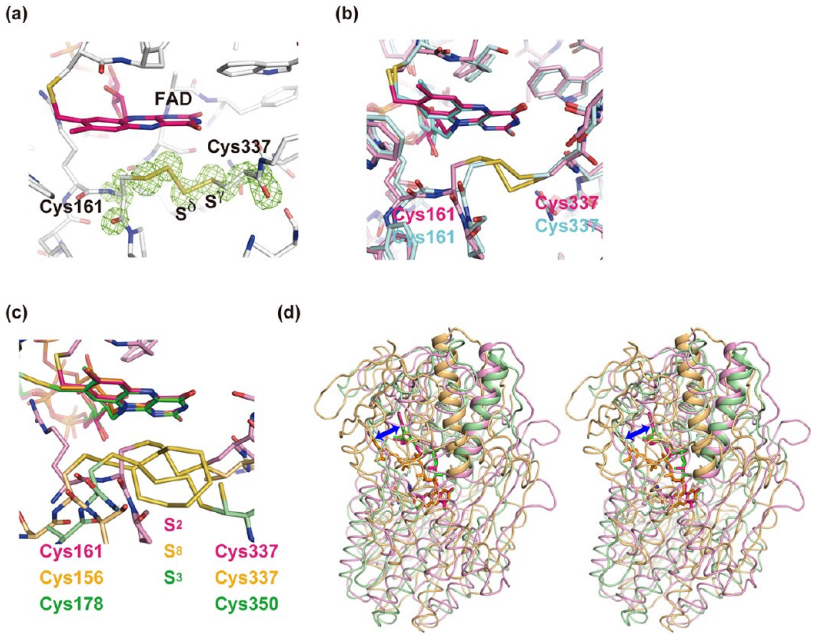

Figure 9. Environment of the FAD in FccB. (a) The $F_o - F_c$ omit map of Cys166 and Cys337 is shown as a green mesh contoured at the 5.0σ level. The positions of S$^{\gamma}$ and S$^{\delta}$ atoms of Cys337 are indicated. (b) Superposition between *Tch. tepidum* (pink) and *Alc. vinosum* (blue). (c) Structural comparison of *Tch. tepidum* FccB (pink), SQR from *Aquifex aeolicus* (orange), and SQR from *Acidianus ambivalens* (green). These structures are superimposed on the FAD isoalloxazine rings. The polysulfur atoms and the cysteine residues are indicated. (d) Stereoview of the structures of *Tch. tepidum* FccB and SQRs with the same color code as in (c). The structures are superposed on the isoalloxazine rings. The α-helices, which have been suggested to influence the redox potentials of FAD, are shown as thick tube models. Positional differences of the adenine moieties are indicated with a blue double-headed arrow.

two cysteine residues were modeled in *Tch. tepidum* flavocytochrome *c*, the distance between the S$^{\gamma}$ atoms of the cysteine residues was 4.90 Å, and two strong peaks in the $F_o - F_c$ electron density map (contour is more than 20σ level) were observed between the two S$^{\gamma}$ atoms. The peaks in the $F_o - F_c$ map were interpreted as two sulfur atoms based on the peak heights and chemical considerations. To fit the two sulfur atoms into the electron densities, two α-mercaptocysteine residues were modeled instead of two cysteine residues (Figure 9a). After refinement of isotropic temperature factors, the two sulfur atoms, S$^{\gamma}$ and S$^{\delta}$, show comparable *B*-factors, 8.2 Å^2 and 10.6 Å^2 in Cys161, and 9.3 Å^2 and 12.0 Å^2 in Cys337. A disulfide bond is formed between the two S$^{\delta}$ atoms with a distance of 2.18 Å. The distance between Cys161 S$^{\gamma}$ and FAD C4A is 3.51 Å. Structures of the residues around Cys161 were different between *Tch. tepidum* and *Alc. vinosum*, but residues around Cys337 fit well to each other (Figure 9b). Recently, the flavocytochrome *c* has been reported to be a member of the sulfide:quinone oxidoreductase (SQR) family.[44] In the crystal structures of SQRs, polysulfur atoms were observed between two cysteine residues adjacent to the isoalloxazine ring of FAD.[45,46] When the isoalloxazine rings were superimposed between FccB and SQRs from *Aquifex aeolicus* (PDB ID: 3HYV)[45] and *Acidianus ambivalens* (PDB ID: 3H8L),[46] the positions of cysteine residues are changed, but polysulfur atoms are located at similar positions on the re-side of FAD (Figure 9c). In addition, the superposition of *Tch. tepidum* FccB and *Acidianus ambivalens* SQR exhibits high similarities in the conformations of the FAD molecules as well as in the structures around the FAD molecules (Figure 9d). However, the FAD molecule in SQR of *Aquifex aeolicus* has different conformations from that of FccB. Since the conformations cause displacement of the adenine moieties, FccB and the SQR from *Aquifex aeolicus* show large structural differences around the isoalloxazine rings of the FAD molecules.

DISCUSSION

In this study, we demonstrated that both Cyt *c*′ and flavocytochrome *c* from *Tch. tepidum* are thermally and structurally much more stable than the corresponding proteins from the closely related mesophilic bacterium *Alc. vinosum*. The enhanced stability can be interpreted on the basis of structural and sequence information. These include the increased number of hydrogen bonds formed between main chain nitrogen and oxygen atoms, more compact structures, and the reduced number of Gly residues. In addition, substitution of many residues with large side chains in the *Alc. vinosum* Cyt *c*′ to the Ala in *Tch. tepidum* Cyt *c*′ is also considered to contribute to the difference in the stability between the two proteins. The reversible nature observed in DSC measurements for the Cyt *c*′ strongly indicates a thermal state transition between the native and the unfolded states. The large values of ΔH and ΔS (Table 1) suggest that *Tch. tepidum* Cyt *c*′ experiences much stronger electrostatic/van der Waals interactions and decreased segmental mobility.[47] Similarly, the ΔH and ΔS for the flavocytochrome *c* of *Tch. tepidum* were also larger than those of *Alc. vinosum*, indicating that the thermal denaturation of *Tch. tepidum* flavocytochrome *c* is entropically more favorable, but enthalpically less favorable, than that of its counterpart. The appearance of two DSC peaks observed for the *Tch. tepidum* flavocytochrome *c* implies that the thermal denaturation involves multiple intermediate states. A molecular chaperone of bacteriophage T4 was reported to show two DSC bands due to the oligomeric states at neutral pH.[48] However, this is not the case since the DSC profile of *Tch. tepidum* flavocytochrome *c* was insensitive to the protein concentration. One of the

dx.doi.org/10.1021/bi3005522 | *Biochemistry* 2012, 51, 6556−6567

possible origins is that the two subunits in this protein denature at different temperatures, as is the case for flagellin.[49] The number of main chain hydrogen bonds is increased in *Tch. tepidum* flavocytochrome *c* compared to that in *Alc. vinosum* flavocytochrome *c*, and almost all of them are located in FccB. This suggests that the difference of thermal stabilities between FccA and FccB in *Tch. tepidum* is larger than that in *Alc. vinosum*. Alternatively, a redox equilibrium of *Tch. tepidum* flavocytochrome *c* may be responsible for the two bands. The present RR analysis of the air-oxidized samples indicated a very small contribution from the reduced form which exhibits an intense DSC band around 79 °C (data not shown). Furthermore, it is reminiscent that this protein shows two distinct redox potentials,[5,7] but the relationship between these two phenomena is unclear. Nevertheless, if each DSC thermogram was assumed to be a convolution of the two bands, the T_m values were estimated to be 70.5 and 76.7 °C for *Tch. tepidum*, and 67.6 and 71.5 °C for *Alc. vinosum*. The respective thermodynamic parameters are given in Supplementary Table S1.

The optimum temperatures for the oxidoreductase activity of flavocytochrome *c* were significantly different, 25 °C for *Alc. vinosum* and 55 °C for *Tch. tepidum*.[5] The activity of *Alc. vinosum* flavocytochrome *c* was completely lost upon incubation at 55 °C. However, the present DSC result showed that the *Alc. vinosum* flavocytochrome *c* did not significantly degrade below 70 °C, suggesting that small alterations in protein structure and/or conformation of the prosthetic groups may significantly affect its activity as temperature increases over 25 °C.

The RR spectra of Cyt *c*′ clearly showed that only ν_{10} bands are different between *Tch. tepidum* and *Alc. vinosum*. The frequencies indicate that the heme iron of *Alc. vinosum* Cyt *c*′ is in an IS state and that of *Tch. tepidum* Cyt *c*′ is in a state of quantum mechanical admixture of IS and HS states.[50] These bands were highly sensitive to the pH (Supplementary Figure S1), where the band at 1635 cm^{-1} was red-shifted to 1625 cm^{-1} with increasing pH. Similar pH dependence of the ν_{10} modes was also observed for *Alc. vinosum* Cyt *c*′ (data not shown) and other cytochromes *c*′ from *Rsp. molischianum* [50] and *Rba. capsulatus*.[51] These results indicate that the pH-induced changes in the ligand field strength are responsible for the difference in the equilibrium state of both spin species.[52] Structural properties contributing to the spin states of the heme iron have been investigated using the high resolution structure of *Rubrivivax gelatinosus* Cyt *c*′.[53] The displacement of the iron atom from heme plane has been reported to bring about a change in the spin states. *Tch. tepidum* Cyt *c*′ shows a smaller iron displacement than *Alc. vinosum* Cyt *c*′ with the deviations of 0.20 Å and 0.19 Å in monomer A and B, respectively. The extent of the displacement may depend on the crystallization conditions, where an acidic buffer at pH 4.0 was used in *Tch. tepidum* and a neutral buffer at pH 7.0 in *Alc. vinosum*.[20] Protonation of the His125 at lower pH reduces the ligand field strength, and as a consequence, the iron atom is less attracted to His125. The pH-dependence is also observed in the hydrogen bond between the His125 and a water molecule. In *Alc. vinosum* Cyt *c*′, His125 and the water molecule show closer contacts (2.74 Å and 2.87 Å in monomer A and B) compared to those in the *Tch. tepidum* Cyt *c*′ (2.95 Å and 2.93 Å in monomer A and B). The distance of hydrogen bond is correlated with the displacement of the heme iron as observed in *Rubrivivax gelatinosus* Cyt *c*′. These structural differences also support the results that the ligand field strength of His125 is sensitive to the conditions of the surrounding solution.

The present result in the RR spectra of *Tch. tepidum* Cyt *c*′ is similar to that of *Rsp. molischianum* Cyt *c*′ in which the IS and HS states were distributed almost equally.[50] However, the IS state has more population in *Rba. sphaeroides* and *Alc. vinosum* cytochromes *c*′. The difference was attributed to the change in axial ligand field strength of the His125, which may be modulated by an adjacent basic residue (Lys or Arg) through electrostatic interactions and imidazole rotation.[50,52] All the cytochromes *c*′ described above have a conserved basic residue at position 129 (Supplementary Figure S2). *Tch. tepidum* and *Rsp. molischianum* cytochromes *c*′ further possess an Asp residue at the C-terminus. The structure of *Tch. tepidum* Cyt *c*′ showed that the Asp131 residue forms a hydrogen bond with Arg129. Although the interaction between Arg129 and Asp131 may depend on the crystal packing in *Tch. tepidum* Cyt *c*′ (Figure 6a,b), these residues can make contacts either directly or indirectly through the solvent molecules. Furthermore, the crystal structure suggests that Arg72 of *Tch. tepidum* Cyt *c*′ is also involved in the ligand field strength of His125 through interaction with Arg129 (Figure 6c). In *Rba. capsulatus* Cyt *c*′, ligand binding to the sixth site of heme iron induces movement of the Glu69 located at the corresponding position of Arg72 in *Tch. tepidum* Cyt *c*′.[54] Therefore, the Arg72 may affect the ligand field strength of His125 when a ligand binds to the sixth coordinate site of the heme iron. Recently, the Arg124 residue in *Alcaligenes xylosoxidans* Cyt *c*′ has been proposed to regulate the NO-binding to the proximal binding site.[55] The NO molecule replaces the axial ligand His120 when it binds to the heme iron. A π−cation interaction may occur between the axial His120 and the adjacent Arg124 side chains with a distance of 3.5 Å. The RR study of several Arg124 mutants did not show significant differences either in the porphyrin conformation or Fe−His interactions in their reduced states,[55] indicating that physicochemical properties of the ferrous cytochromes *c*′ are little affected by the Arg124 mutation. In *Tch. tepidum* Cyt *c*′, the Arg129 is located at the similar position of Arg124 in *Alcaligenes xylosoxidans* Cyt *c*′, and there is a closer contact between the Arg129 and His125 with a distance of ∼3.3 Å. In addition, the IS/HS equilibrium of the *Tch. tepidum* Cyt *c*′ is sensitive to the Arg129 mutation (unpublished results). Therefore, both the Arg129 and Arg72 may also influence the heme properties through the proximal His125 in the ferric Cyt *c*′.

The RR bands observed for flavocytochromes *c* are mainly ascribed to the heme vibrational modes, and are almost identical between *Tch. tepidum* and *Alc. vinosum*. This is consistent with the RR results using Soret band excitation[5] and indicates a quite similar environment of the heme centers in both species. It was reported that the two hemes in *Alc. vinosum* flavocytochrome *c* were not equivalent in terms of axial ligation and accessibility to the bulk medium.[56] However, the RR spectra for both flavocytochromes *c* did not show significant pH-dependence at physiological conditions (data not shown). In the crystal structure, water molecules were only found around the His105 ligand, and the nearest water is located at the position perpendicular to the His105 imidazole plane (Figure 8b). This water molecule may have very weak effects on the coordination of His105. These results support that the properties of the heme irons in flavocytochrome *c* are insensitive to the environmental changes, in contrast to the Cyt *c*′ where the heme binding site exists at the solvent-exposed

dx.doi.org/10.1021/bi3005522 | *Biochemistry* 2012, 51, 6556−6567

C-terminal area. It was noted that the flavocytochrome *c* spectra measured under the present condition show some characteristics of the reduced state, implying that the air-oxidized flavocytochrome *c* may contain a small amount of reduced species (see below).

The coordination distances from the axial ligands to the heme iron in *Tch. tepidum* flavocytochrome *c* do not show significant differences between the N-terminal heme 1 and the C-terminal heme 2, while the distance is longer for the N-terminal heme group in the Cyt c_4. The His15 of heme 1 ligand is hydrogen bonded to Pro27 and the His105 of heme 2 ligand to His119 in FccA (Figure 8a,b). Whereas in Cyt c_4, the histidine ligands of both hemes are hydrogen bonded to the conserved proline residues.[42,43] The hydrogen bond between His15 and Pro27 is probably modulated by FccA−FccB interactions because the Ser26 next to Pro27 forms a hydrogen bond with Ser390 in FccB. The characteristics in hydrogen bonds may influence electronic properties of the heme iron.[57] On the other hand, the hydrogen bonds involving propionates and amino acids have been proposed to be important for the electron transfer between the two heme groups in Cyt c_4.[42] In the FccA, part of the hydrogen bonds around the propionate groups are lost, and a water molecule is substituted for the hydroxyl group of tyrosine residue to participate in the hydrogen bond network with the propionates of the two heme groups (Figure 8d). The features in the interheme region suggest that solution conditions may affect the reduction potentials and electron transfer rate[57] because this water molecule is linked to the solvent region on the exterior of FccB.

The electron density map of *Tch. tepidum* flavocytochrome *c* revealed unambiguous electron densities of disulfur atoms at the active site near FAD. The absence of a disulfide bond and presence of extra electron density near Cys337 were observed in a preliminary crystal structure of flavocytochrome *c* from *Halochromatium salexigens*.[58] The position of disulfur atoms is analogous to that of the polysulfur observed in SQRs (Figure 9c). Therefore, flavocytochrome *c* possibly follows the same mechanism of sulfide oxidation as proposed for SQR.[45] The presence of disulfur indicates that the air-oxidized flavocytochrome *c* was not in the fully oxidized state, in agreement with the observation of RR measurement. The oxidation state of a crystal previously used for structure determination of *Alc. vinosum* flavocytochrome *c* was not mentioned in the literature.[59] In addition, although the conformations of the Cys161 are in the outlier region of the Ramachandran plot, the electron densities of the cysteine residues (Cys161 and Cys337) could not be examined due to the absence of structure factor in PDB. If the crystal structure previously determined represents the truly oxidized state, it means that there is a structural difference caused by the sulfide oxidation between *Tch. tepidum* and *Alc. vinosum*. Because Cys161 is in a loop region and Cys337 is located at a β-sheet, the Cys161 may move toward Cys337 after a sulfide adduct approaches the FAD isoalloxazine ring. Although the *in vivo* function of flavocytochrome *c* is still unclear, the presence of disulfur at the FAD binding site strongly suggests that flavocytochrome *c* is involved in the sulfide oxidation *in vivo* as the crystal was obtained using the sample purified from fresh *Tch. tepidum* cells. In contrast to the similarities of polysulfur atoms, the SQR from *Aquifex aeolicus* shows structural differences around the isoalloxazine ring from FccB or the SQR from *Acidianus ambivalens*. The dissimilar orientations of the helix dipoles relative to the isoalloxazine rings may have effects on the redox potentials of FAD.[60] In sulfide oxidation process, the elemental sulfur atoms have been suggested to be transferred through interaction between the flavocytochrome *c* and the SoxYZ complex.[61] The SoxYZ complex carries multiple sulfur compounds and its crystal structure shows that the C-terminal cysteine residue of SoxY binds the sulfur compounds. Homology modeling with SoxYZ shows that the C-terminal cysteine residue of SoxY is located at the highly conserved region on the surface of the complex (Supplementary Figure S3). The C-terminal region is relatively hydrophobic and surrounded by positively charged surfaces. Flavocytochrome *c* has the highly conserved surface around the cavity connecting to the isoalloxazine ring. Since the cavity consists of positively charged surface, an electrostatic repulsion may contribute to maintaining a proper orientation of the SoxYZ when it interacts with the flavocytochrome *c*.

■ ASSOCIATED CONTENT

Ⓢ Supporting Information

Thermodynamic parameters obtained by deconvolution of the DSC bands for the *Tch. tepidum* and *Alc. vinosum* flavocytochromes *c* (Table S1). Changes of the RR spectra of the *Tch. tepidum* Cyt *c′* as a function of pH (Figure S1). Alignment of the amino acid sequences of C-terminal regions for the cytochromes *c′* from several photosynthetic bacteria (Figure S2). A possible interaction site between the flavocytochrome *c* and SoxYZ (Figure S3). This material is available free of charge via the Internet at http://pubs.acs.org.

Accession Codes

Coordinates of the crystal structures of the *Tch. tepidum* cytochrome *c′* and flavocytochrome *c* have been deposited in the Protein Data Bank under accession codes 3VRC and 3VRD, respectively.

■ AUTHOR INFORMATION

Corresponding Author

*(Z.-Y.W.) Telephone and fax +81-29-228-8352. E-mail: wang@mx.ibaraki.ac.jp. (K.M.) Telephone +81-75-753-4029. Fax +81-75-753-4032. E-mail: miki@kuchem.kyoto-u.ac.jp.

Author Contributions

#These authors contributed equally to this work.

Funding

This work was supported by grants-in-aid for scientific research on priority areas "Structures of Biological Macromolecular Assemblies" from the Ministry of Education, Culture, Sports, Science and Technology of Japan, and by The Kurata Memorial Hitachi Science and Technology Foundation.

Notes

The authors declare no competing financial interest.

■ ACKNOWLEDGMENTS

We thank M. Takasaki, R. Genji, M. Ushijima, A. Kimura, and A. Maruyama for their technical assistance. This work was performed under the approval of the Photon Factory Program Advisory Committee (Proposal No. 2007G585), and we thank the beamline staff for their help in data collection.

■ ABBREVIATIONS USED

cycP, gene encoding the cytochrome *c′*; CycP, gene product of *cycP*; Cyt, cytochrome; DSC, differential scanning calorimetry; FAD, flavin adenine dinucleotide; *fccA* and *fccB*, genes encoding the diheme-binding subunit and FAD-binding subunit of flavocytochrome *c*, respectively; FccA and FccB, gene products

of *fccA* and *fccB*, respectively; GuHCl, guanidine hydrochloride; HiPIP, high-potential iron−sulfur protein; IS, intermediate spin; HS, high spin; LH1-RC, light-harvesting-reaction center core complex; NMR, nuclear magnetic resonance; rms, root-mean-square; RR, resonance Raman; SQR, sulfide:quinone oxidoreductase

REFERENCES

(1) Madigan, M. T. (1984) A novel photosynthetic bacterium isolated from a Yellowstone hot spring. *Science 225*, 313−315.

(2) Kimura, Y., Yu, L.-J., Hirano, Y., Suzuki, H., and Wang, Z.-Y. (2009) Calcium ions are required for the enhanced thermal stability of the light-harvesting-reaction center core complex from thermophilic purple sulfur bacterium *Thermochromatium tepidum*. *J. Biol. Chem. 284*, 93−99.

(3) Heda, G. D., and Madigan, M. T. (1988) Thermal properties and oxygenase activity of ribulose-1,5-bisphosphate carboxylase from the thermophilic purple bacterium, *Chromatium tepidum*. *FEMS Microbiol. Lett. 51*, 45−50.

(4) Heda, G. D., and Madigan, M. T. (1989) Purification and characterization of the thermostable ribulose-1,5-bisphosphate carboxylate/oxygenase from the thermophilic purple bacterium *Chromatium tepidum*. *Eur. J. Biochem. 184*, 313−319.

(5) Castillo, M. C. G., Lou, B.-S., Ondrias, M. R., Robertson, D. E., and Knaff, D. B. (1994) Characterization of flavocytochrome c_{552} from the thermophilic photosynthetic bacterium *Chromatium tepidum*. *Arch. Biochem. Biophys. 315*, 262−266.

(6) Moulis, J.-M., Scherrer, N., Gagnon, J., Forest, E., Petillot, Y., and Garcia, D. (1993) Primary structure of *Chromatium tepidum* high-potential iron-sulfur protein in relation to thermal denaturation. *Arch. Biochem. Biophys. 305*, 186−192.

(7) Kobayashi, M., Saito, T., Takahashi, K., Wang, Z.-Y., and Nozawa, T. (2005) Electronic properties and thermal stability of soluble redox proteins from a thermophilic purple sulfur photosynthetic bacterium. *Thermochromatium tepidum*. *Bull. Chem. Soc. Jpn. 78*, 2164−2170.

(8) Liu, L.-J., Nogi, T., Kobayashi, M., Nozawa, T., and Miki, K. (2002) Ultrahigh-resolution structure of high-potential iron-sulfur protein from *Thermochromatium tepidum*. *Acta Crystallogr. D58*, 1085−1091.

(9) Weiss, R., Gold, A., and Terner, J. (2006) Cytochrome *c*′: Biological models for the *S* = 3/2, 5/2 spin-state admixture? *Chem. Rev. 106*, 2550−2579.

(10) Moore, G. R., and Pettigrew, G. W. (1990) *Cytochromes c: Evolutionary, Structural and Physicochemical Aspects*, Springer-Verlag, Berlin Heidelberg.

(11) Meyer, T. E., and Cusanovich, M. A. (2003) Discovery and characterization of electron transfer proteins in the photosynthetic bacteria. *Photosynth. Res. 76*, 111−126.

(12) Cusanovich, M. A., and Gibson, Q. H. (1973) Anomalous ligand binding by a class of high spin *c*-type cytochromes. *J. Biol. Chem. 248*, 822−834.

(13) Rubinow, S. C., and Kassner, R. J. (1984) Cytochromes *c*′ in their reaction with ethyl isocyanide. *Biochemistry 23*, 2590−2595.

(14) Kassner, R. J. (1991) Ligand binding properties of cytochromes *c*′. *Biochim. Biophys. Acta 1058*, 8−12.

(15) Yoshimura, T., Fujii, S., Kamada, H., Yamaguchi, K., Suzuki, S., Shidara, S., and Takakuwa, S. (1996) Spectroscopic characterization of nitrosylheme in nitric oxide complexes of ferric and ferrous cytochrome *c*′ from photosynthetic bacteria. *Biochim. Biophys. Acta 1292*, 39−46.

(16) Kassner, R. J., Kykta, M. G., and Cusanovich, M. A. (1985) Binding of cyanide to cytochrome *c*′ from *Chromatium vinosum*. *Biochim. Biophys. Acta 831*, 155−158.

(17) Suzuki, S., Nakahara, A., Yoshimura, T., Iwasaki, H., Shidara, S., and Matsubara, T. (1988) Spectral properties of carbon monoxide or cyanide complexes of cytochromes *c*′ from denitrifying bacteria. *Inorg. Chim. Acta 153*, 227−233.

(18) Ambler, R. P., Bartsch, R. G., Daniel, M., Kamen, M. D., McLellan, L., Meyer, T. E., and van Beeumen, J. (1981) Amino acid sequences of bacterial cytochromes *c*′ and *c*-556. *Proc. Natl. Acad. Sci. USA 78*, 6854−6857.

(19) Shibata, N., Iba, S., Misaki, S., Meyer, T. E., Bartsch, R. G., Cusanovich, M. A., Morimoto, Y., Higuchi, Y., and Yasuoka, N. (1998) Basis for monomer stabilization in *Rhodopseudomonas palustris* cytochrome *c*′ derived from the crystal structure. *J. Mol. Biol. 284*, 751−760.

(20) Ren, Z., Meyer, T., and McRee, D. E. (1993) Atomic structure of a cytochrome *c*′ with an unusual ligand-controlled dimer dissociation at 1.8 Å resolution. *J. Mol. Biol. 234*, 433−445.

(21) Fukumori, Y., and Yamanaka, T. (1979) Flavocytochrome *c* of *Chromatium vinosum*. *J. Biochem. 85*, 1405−1414.

(22) Dahl, C. (2008) Inorganic sulfur compounds as electron donors in purple sulfur bacteria, in *Sulfur Metabolism in Phototrophic Organisms* (Hell, R., Dahl, C., Knaff, D., Leustek, T., Eds.) pp 289−317, Springer, Dordrecht, The Netherlands.

(23) Frigaard, N.-U., Bryant, D. A. (2008) Genomic insights into the sulfur metabolism of phototrophic green sulfur bacteria, in *Sulfur Metabolism in Phototrophic Organisms* (Hell, R., Dahl, C., Knaff, D., Leustek, T., Eds.) pp 337−355, Springer, Dordrecht, The Netherlands.

(24) Reinartz, M., Tschäpe, J., Brüser, T., Trüper, H. G., and Dahl, C. (1998) Sulfide oxidation in the phototrophic sulfur bacterium *Chromatium vinosum*. *Arch. Microbiol. 170*, 59−68.

(25) Chen, Z.-w., Koh, M., van Driessche, G., van Beeumen, J. J., Bartsch, R. G., Meyer, T. E., Cusanovich, M. A., and Mathews, F. S. (1994) The structure of flavocytochrome *c* sulfide dehydrogenase from a purple photosynthetic bacterium. *Science 266*, 430−432.

(26) Fathir, I., Tanaka, K., Yoza, K., Kojima, A., Kobayashi, M., Wang, Z.-Y., Lottspeich, F., and Nozawa, T. (1997) The genes coding for the L, M and cytochrome subunits of the photosynthetic reaction center from the thermophilic purple sulfur bacterium *Chromatium tepidum*. *Photosynth. Res. 51*, 71−82.

(27) Even, M. T., Kassner, R. J., Dolata, M., Meyer, T. E., and Cusanovich, M. A. (1995) Molecular cloning and sequencing of cytochrome *c*′ from the phototrophic purple sulfur bacterium *Chromatium vinosum*. *Biochim. Biophys. Acta 1231*, 220−222.

(28) Sekine, F., Horiguch, K., Kashino, Y., Shimizu, Y., Yu, L.-J., Kobayashi, M., and Wang, Z.-Y. (2012) Gene sequencing and characterization of the light-harvesting complex 2 from thermophilic purple sulfur bacterium *Thermochromatium tepidum*. *Photosynth. Res. 111*, 9−18.

(29) Dolata, M. M., van Beeumen, J. J., Ambler, R. P., Meyer, T. E., and Cusanovich, M. A. (1993) Nucleotide sequence of the heme subunit of flavocytochrome *c* from the purple phototrophic bacterium, *Chromatium vinosum*. *J. Biol. Chem. 268*, 14426−14431.

(30) Wang, Z.-Y., Shimonaga, M., Suzuki, H., Kobayashi, M., and Nozawa, T. (2003) Purification and characterization of the polypeptides of core light-harvesting complexes from purple sulfur bacteria. *Photosynth. Res. 78*, 133−141.

(31) Higuchi, M., Hirano, Y., Kimura, Y., Oh-oka, H., Miki, K., and Wang, Z.-Y. (2009) Overexpression, characterization, and crystallization of the functional domain of cytochrome c_z from *Chlorobium tepidum*. *Photosynth. Res. 102*, 77−84.

(32) Privalov, G., Kavina, V., Freire, E., and Privalov, P. L. (1995) Precise scanning calorimeter for studying thermal-properties of biological macromolecules in dilute-solution. *Anal. Biochem. 232*, 79−85.

(33) Otwinowski, Z., and Minor, W. (1997) Processing of X-ray diffraction data collected in oscillation mode, in *Methods in Enzymology. Macromolecular crystallography Part A* (Charles, W., Carter, J., Robert, M. S., Eds.) pp 307−326, Academic Press, New York.

(34) Vagin, A., and Teplyakov, A. (1997) MOLREP: an automated program for molecular replacement. *J. Appl. Crystallogr. 30*, 1022−1025.

(35) Murshudov, G. N., Levedev, A., Vagin, A. A., Wilson, K. S., and Dodson, E. J. (1999) Efficient anisotropic refinement of macromolecular structure using FFT. *Acta Crystallogr. D55*, 247−255.
(36) Emsley, P., Lohkamp, B., Scott, W. G., and Cowtan, K. (2010) Features and development of. *Coot. Acta Cryst. D66*, 486−501.
(37) Davis, I. W., Leaver-Fay, A., Chen, V. B., Block, J. N., Kapral, G. J., Wang, X., Murray, L. W., Arendall, W. B., III, Snoeyink, J., Richardson, J. S., and Richardoson, D. C. (2007) MolProbity: all-atom and structure validation for proteins and nucleic acids. *Nucleic Acids Res. 35*, W375−383.
(38) DeLano, W. L. (2004) The PyMOL molecular graphics system, DeLano Scientific, LCC, San Carlos, CA, USA.
(39) Spiro, T. G., and Strekas, T. C. (1974) Resonance Raman spectra of heme proteins. Effects of oxidation and spin state. *J. Am. Chem. Soc. 96*, 338−345.
(40) Desbois, A. (1994) Resonance Raman spectroscopy of c-type cytochromes. *Biochimie 76*, 693−707.
(41) Robinson-Rechavi, M., Alibes, A., and Godzik, A. (2006) Contribution of electrostatic interactions, compactness and quaternary structure to protein thermostability: lessons from structural genomics of *Thermotoga maritima*. *J. Mol. Biol. 356*, 547−557.
(42) Kadziola, A., and Larsen, S. (1997) Crystal structure of the dihaem cytochrome c_4 from *Pseudomonas stutzeri* determined at 2.2 Å resolution. *Structure 5*, 203−216.
(43) Abergel, C., Nitschke, W., Malarte, G., Bruschi, M., Claverie, J.-M., and Giudici-Orticoni, M.-T. (2003) The structure of *Acidithiobacillus ferrooxidans* c_4-cytochrome: a model complex-induced electron transfer tuning. *Structure 11*, 547−555.
(44) Marcia, M., Ermler, U., Peng, G., and Michel, H. (2010) A new structure-based classification of sulfide:quinone oxidoreductases. *Proteins 78*, 1073−1083.
(45) Marcia, M., Ermler, U., Peng, G., and Michel, H. (2009) The structure of *Aquifex aeolicus* sulfide:quinone oxidoreductase, a basis to understand sulfide detoxification and respiration. *Proc. Natl. Acad. Sci. U. S. A. 106*, 9625−9630.
(46) Brito, J. A., Sousa, F. L., Stelter, M., Bandeiras, T. M., Vonrhein, C., Teixeira, M., Pereira, M., and Archer, M. (2009) Structural and functional insights into sulfide:quinone oxidoreductase. *Biochemistry 48*, 5613−5622.
(47) Lett, C. M., Berghuis, A. M., Frey, H. E., Lepock, J. R., and Guillemette, J. G. (1996) The role of a conserved water molecule in the redox-dependent thermal stability of iso-1-cytochrome *c*. *J. Biol. Chem. 271*, 29088−29093.
(48) Ali, S. A., Iwabuchi, N., Matsui, T., Hirota, K., Kidokoro, S., Arai, M., Kuwajima, K., Schuck, P., and Arisaka, F. (2003) Reversible and fast association equilibria of a molecular chaperone, gp57A, of bacteriophage T4. *Biophys. J. 85*, 2606−2618.
(49) Vonderviszt, F., Uedaira, H., Kidokoro, S. I., and Namba, K. (1990) Structural organization of flagellin. *J. Mol. Biol. 214*, 97−104.
(50) Othman, S., Richaud, P., Vermeglio, A., and Desbois, A. (1996) Evidence for a proximal histidine interaction in the structure of cytochromes *c′* in solution: A resonance Raman study. *Biochemistry 35*, 9224−9234.
(51) Huston, W. M., Andrew, C. R., Servid, A. E., McKay, A. L., Leech, A. P., Butler, C. S., and Moir, J. W. B. (2006) Heterologous overexpression and purification of cytochrome *c′* from *Rhodobacter capsulatus* and a mutant (K42E) in dimerization region. Mutation does not alter oligomerization but impacts the heme iron spin state and nitric oxide binding properties. *Biochemistry 45*, 4388−4395.
(52) Weber, P. C. (1982) Correlations between structural and spectroscopic properties of the high-spin heme protein cytochrome-*c′*. *Biochemistry 21*, 5116−5119.
(53) Benini, S., Rypnoewski, W. R., Wilson, K. S., and Ciurli, S. (2008) High resolution crystal structure of *Rubrivivax gelatinosus* cytochrome *c′*. *J. Inorg. Biochem. 102*, 1322−1328.
(54) Tahirov, T. H., Misaki, S., Meyer, T. E., Cusanovich, M. A., Higuchi, Y., and Yasuoka, N. (1996) Concerted movement of side chains in the haem vicinity observed on ligand binding in cytochrome *c′* from *Rhodobacter capsulatus*. *Nat. Struct. Biol. 3*, 459−464.
(55) Hough, M. A., Antonyuk, S. V., Barbieri, S., Rustage, N., McKay, A. L., Servid, A. E., Eady, R. R., Andrew, C. R., and Hasnain, S. S. (2010) Distal-to-proximal NO conversion in hemoproteins: the role of the proximal pocket. *J. Mol. Biol. 405*, 395−409.
(56) Castillo, M. C. G., Finnegan, M. G., Conover, R. C., Knaff, D. B., and Johnson, M. K. (1994) Spectroscopic characterization of flavocytochrome *c*-552 from the photosynthetic purple sulfur bacterium *Chromatium vinosum*. *Biochim. Biophys. Acta 1184*, 273−278.
(57) Andersen, N. H., Christensen, H. E. M., Iversen, G., Norgaard, A., Scharnagl, C., Thuesen, M. H., Ulstrup, J. (2001) Cytochrome c_4, in *Handbook of Metalloproteins* (Messerschmidt, A., Huber, R., Poulos, T., Wieghardt, K., Eds.), pp 100−109, John Wiley & Sons, Chichester, England.
(58) Leys, D., Smet, L. D., Beeumen, J. J. V., Meyer, T. E., Cusanovich, M. A. (2002) Preliminary crystal structure of a flavocytochrome c-sulfide dehydrogenase (FCSD) from the halophilic phototrophic sulfur bacterium, *Halochromatium salexigens*, in *Flavin and Flavoproteins 2002* (Chapman, S., Perham, R., Scrutton, N., Eds.) pp 83−87, Rudolf Weber, Agency for Scientific Publications, Berlin, Germany, St. John's College, University of Cambridge, UK.
(59) Salemme, F. R. (1982) Preliminary X-ray studies on *Chromatium vinosum* flavocytochrome c_{552}. *J. Mol. Biol. 159*, 551−552.
(60) Heuts, D. P. H. M., Scrutton, N. S., McIntire, W. S., and Fraaije, M. W. (2009) What's in a covalent bond? On the role and formation of covalently bound flavin cofactors. *FEBS J. 276*, 3405−3427.
(61) Sauvé, V., Bruno, S., Berks, B. C., and Hemmings, A. M. (2007) The SoxYZ complex carries sulfur cycle intermediates on a peptide swinging arm. *J. Biol. Chem. 282*, 23194−23204.